MASTER THESIS PROJECT

Effect of atomic and molecular hydrogen on the reduction process of ruthenium dioxide

Ester Pérez Penco

Examiner and supervisor: Roland Bliem
Daily supervisor: Stefan van Vliet
Second reviewer: Paul Planken

MSc Physics and Astronomy: Advanced Matter and Energy Physics
2021-2022

Universiteit van Amsterdam
ARCNL

UNIVERSITEIT VAN AMSTERDAM

Abstract

Gaining insights into the reduction process of ruthenium dioxide by atomic hydrogen is relevant for the optimization of the lifetime of the optics of extreme ultraviolet nanolithography machines. This thesis reports an in situ X-ray photoelectron spectroscopy (XPS) study of the different effect that atomic vs molecular hydrogen has on the reduction of ruthenium dioxide. The results presented in this research demonstrate that reduction of RuO_2 using H* leads to a more effective and faster reduction of the oxide layer than through H_2. A detailed study of the evolution of the oxygen species involved in this reaction, oxide, hydroxide, and adsorbed water is reported. A systematic difference of the evolution of these 3 oxygen species during reduction with H* and H_2 is identified.

Contents

1. Introduction

Apple's latest release, IPhone 13, features the A15 bionic chip. This processor consists of *15 billion* transistors in just 1 cm^2. The number of transistors in the newest technology devices exceeds the expectations held when the semi-conductor industry started to develop 60 years ago [1]. Moore's law, introduced by the co-founder of Intel Gordon Moore, encapsulates an exponential growth. It states that the number of transistors in a dense integrated circuit (IC) doubles every two years [2]. Moore's law dates to 1965 and it is still very relevant up to this day [3]. However, the death of this law has been announced several times over the course of time. Stating that features could not be physically scaled down any further and hence the number of transistors in the chip could not be increased.

Nevertheless, over the years, technology has managed to keep pushing this limit further . This has been possible by consistently scaling down the linear dimensions of transistors. The growth law of the *number* of transistors inside a chip goes irrevocably hand by hand with a shrinking of its *dimension* law. Every 4 years the dimensions shrink by a factor of 2 [4]. Scaling down in the x and in the y axis implies the quadruplication of the number of elements per unit area every 4 years. Such shrinking rhythm implies that the transistor industry is inevitably approaching the atomic dimension.

There is constant pressure and demand on technology to keep up to with the scaling law. In other words, if technology does not keep pushing further this dimension limit, technology will simply not be *physically* able of advancing further. The focus of the semi-conductor industry is set towards developing new technologies to keep scaling down. At the end of the day this is a question that comes down to very fundamental and complex physics.

Therefore, how can industry keep up with Moore's law?

The exponential scaling down of technology is possible by virtues of a technology that, by concept, has not changed in the last 50 years, Lithography.

1.1 Lithography

Lithography is a photochemical process that allows to imprint features on to a substrate. It consists of several steps. First, light is shone through a mask containing the desired chip pattern onto a silicon wafer [5,6]. The wafer is coated with a photoresist that will suffer a chemical change when exposed to light. Next step is chemical development to uncover the pattern. Etching of the silicon away and ion implantation follows. These steps are performed to manipulate the properties of the exposed silicon in order to gain functionality for the device. Finally, the remaining photoresist is stripped away, a new photoresist film is applied and the cycle is repeated. To create a computer chip the cycle is performed 50-100 times.

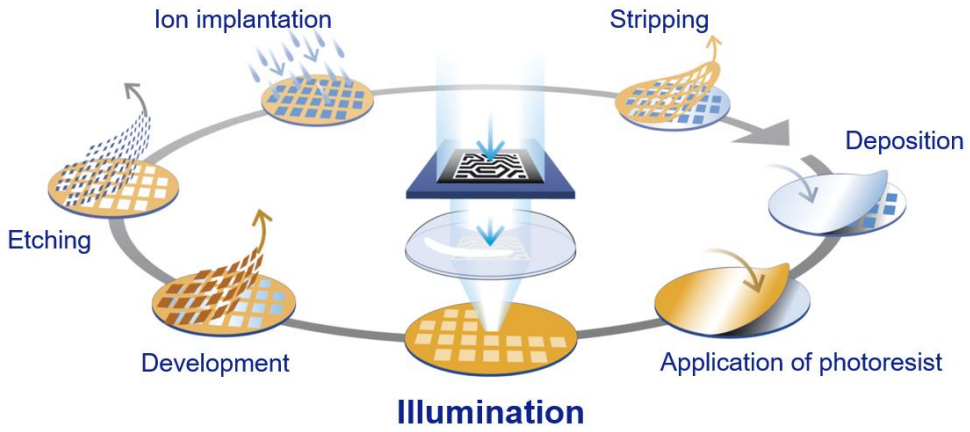

Figure 1: Nanolithography process [7].

The smallest lithography-printable feature is dictated by the Abbe diffraction limit [4], which ca be expressed as:

$$CD = k_1 \frac{\lambda}{NA} \quad (1)$$

Where *CD* is known as the critical dimension (smallest printable feature), k_1 a parameter that contains litho-process related information, such as the mask and resist. λ is the wavelength of light in vacuum and *NA* is the numerical aperture of the optics. It is clear from Abbe's formula that both the numerical aperture and the wavelength play a key role in the scaling down of the critical dimension. The revolutionary step that was taken by the semi-conductor industry was the reduction of the wavelength, from 193 nm to 13.5 nm, resulting in Extreme Ultraviolet Lithography (EUVL) [4]. This advance was made possible by close collaboration of high-tech companies and fundamental scientific research.

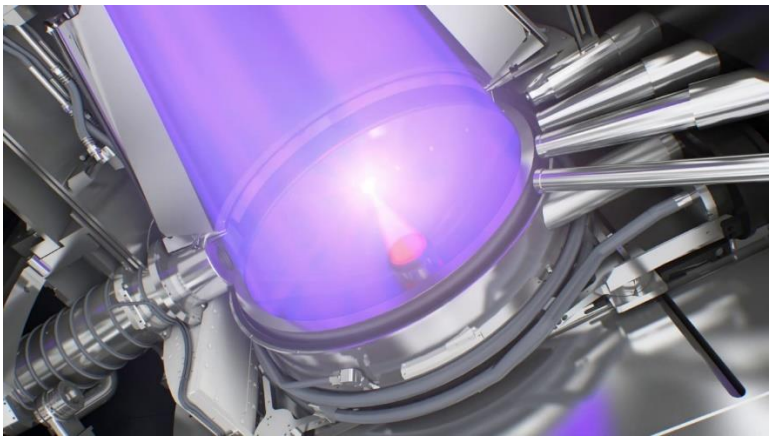

Figure 2: Extreme ultraviolet (EUV) light source vessel in ASML's TWINSCAN NXE:3400 lithography machine. *Image from ASML.*

1.2 Research question

The development of the technology that enabled to keep scaling down demanded to almost re-define the previously employed lithography systems. One of the added complexity factors was working with EUV light due to its extremely high absorption index [8]. In order to work with such short wavelength, reflective multilayer optics in a near-vacuum H_2 background gas were introduced [9, 10].

Due to contaminant agents present inside the machine, the lifetime of these optics is one of the major challenges that EUVL faces. To minimize this problem a ruthenium (Ru) coating is used as an oxidation resistant capping layer for the multilayer mirrors [11]. Nevertheless, overtime oxidation of this Ru protective layer leads to decrease in the reflectivity and, hence, a shorter lifespan of the optics. Removal of the ruthenium oxide layer is key to optimizing the performance of EUVL machines.

The reducing environment inside the machine is employed to fight the effect of the contaminants and maintain self-cleaning conditions for the optics [9]. As a consequence, reduction of the oxide layer through the exposure to hydrogen should occur [10]. However, there is scarce knowledge about the process taking place. Specifically, it is not completely understood the differences between the effect of molecular and atomic hydrogen in the reduction of the oxide [12-14]. Gaining insights into the stages of the reduction and its optimal conditions would contribute to the optimization of the optics of the EUV machines.

This leads to my research question:

What is the difference between the effect of atomic vs molecular hydrogen on the reduction process of ruthenium dioxide?

2 Theoretical background

2.1 Reduction of ruthenium dioxide

Reduction is the electrochemical process by which the atom or ion gains electrons. This implies the decrease in its oxidation state. The reduction of metal oxides by hydrogen follows the reaction:

$$MO_x + xH_2 \rightarrow M + xH_2O \ (2)$$

Specifically, the aim of this master thesis will be set towards achieving a deeper understanding of the reduction process of ruthenium dioxide with hydrogen radicals:

$$RuO_2 + 4H^* \rightarrow Ru + 2H_2O \ (3)$$

In an oxygen-rich environment, ruthenium single crystal (Ru(0001)) oxidizes forming a rutile crystal structure that grows epitaxially on the metal surface forming RuO_2(110), figure 3. Exposure to hydrogen will induce the reduction of this oxide layer following reaction (3).
The incoming hydrogen atoms will bond with the bridging oxygen species on the RuO_2 surface, forming a hydroxyl group (O-H) [13,15]. Upon the pickup of another H, the formation of a water molecule takes place. Re-accommodation of the H_2O in the lattice follows. In this new location it is energetically more favorable to be thermally desorbed, 300K (27ºC) is enough for this process to take place. This process will trigger an oxygen vacancy gradient perpendicular to the surface, inducing oxygen diffusion from the bulk of the RuO_2 towards the surface. The creation of such oxygen vacancies is crucial for the reduction process [16-17]. This exchange mechanism will keep driving the reduction process until the oxygen atoms are removed from the surface.

The reduction process varies for molecular (H_2) and atomic (H*) hydrogen [13,14]. Previous research stablishes that the reduction of stoichiometric RuO_2(110) film by molecular hydrogen at pressure of 1×10^{-6} mbar is highly dependent on the temperature . The reduction process between 100-200ºC is characterized by an initial period where reduction does not take place, followed by a fast reduction regime until a constant amount of oxide left. In the range of 200-300 ºC some slow reduction is already observed in the initial stage followed by a fast total reduction of the oxide. Above 300ºC degrees the reduction starts immediately and achieves a fast full reduction [13].

The reduction efficiency of RuO_2(110) film through atomic hydrogen has been reported to be an order of magnitude higher than when reduced with molecular hydrogen under similar conditions [14]. In the temperature range of 60-200ºC reduction with atomic hydrogen starts with an initial slow rate followed by a fast reduction where the majority of the oxide is removed within minutes. Nevertheless, full reduction of the oxide layer in never observed. The reduction by atomic hydrogen becomes less effective in the last stage due to the formation of ruthenium islands that trigger the recombination of the hyhdrogen [14]. Reduction of RuO_2 reported by a higher pressure of hydrogen of 0.13 mbar and a flow rate of 50 scmm still did not lead to complete full reduction [12].
The role that the different oxygen species play in the reduction process is uncertain. Matter that will be targeted in this research.

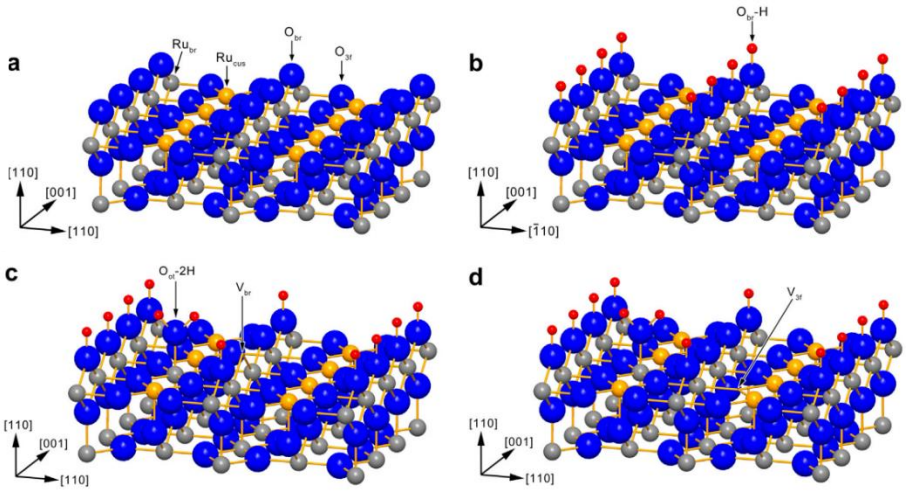

Figure 3: (a) Stoichiometric RuO_2(110) surface with O in blue and Ru in grey and yellow, (b) hydrogenated surface with the O–H groups with hydrogen in red, (c) hydrogen transfer reaction forming adsorbed water vapor species (O–2H) and an oxygen vacancy due to the displacement of the O atom, and (d) formation of a vacancy at the bulk due to the diffusion of an O atom to the surface to fill the vacancy [13].

2.2 X-ray Photoelectron Spectroscopy

X-ray Photoelectron Spectroscopy (XPS) is a surface sensitive spectroscopic technique that allows for surface composition determination. It was introduced in 1960s by Kai Siegbahn in Uppsala, Sweden [19], who would later receive the Nobel Prize in 1981 for this development. It is based in the photoelectric effect formulated by Einstein in 1905 [20], description that awarded him the Nobel Prize in 1921.

The photoelectric effect describes the emission of electrons from a material upon the absorption of electromagnetic radiation. The emitted electrons are called photoelectrons. In XPS, X-rays in the range of 100 eV-10 KeV penetrate onto the sample exciting a photoelectron from the core levels of the atom. This photoelectron will be ejected from the sample with certain kinetic energy encoding information of the atomic species. Such kinetic energy is given by:

$$KE = h\nu - BE - \phi \quad (4)$$

Where *KE* is the kinetic energy of the registered photoelectron, $h\nu$ is the energy of the impinging X-rays, *BE* is binding energy and ϕ the work function.
The binding energy is not only characteristic to each atomic species but also to the oxidation state. Different oxidation states will cause a shift in the binding energy. This effect is due to the screening of the nuclear charge and to the addition of a Madelung term in the electrostatic potential of the crystal field Hamiltonian [21]. Therefore, XPS can be used to determine the sample composition as well as to identify the chemical state of the materials being analyzed.
Exposure to X-rays does not only yield the emission of photoelectrons involved the photoelectric process. The relaxation of the atom after the ejection of a photoelectron implies the filling of the vacancy by an electron at lower binding energy. This electronic recombination will release energy that will provoke the emission of Auger electron with a characteristic energy. The resulting Auger electrons can be detected with XPS and used to further characterize the material composition.

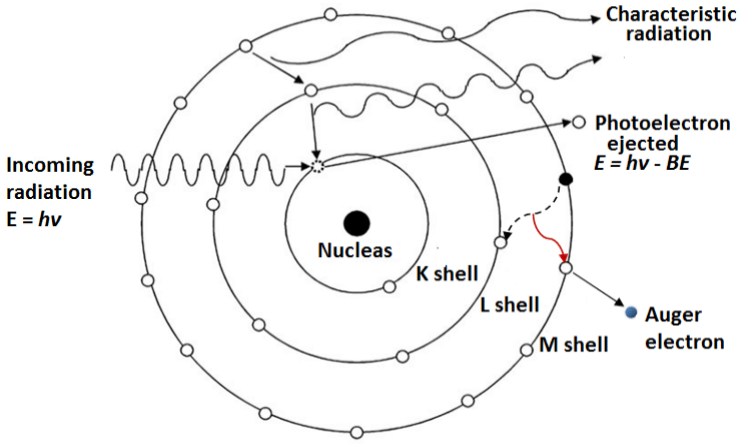

Figure 4: Photoelectric effect diagram [22].

XPS allows to probe the first 5 to 10 nm of the surface of a material. What attributes the surface sensitive characteristic to XPS is the short inelastic mean free path (IMFP) of the photoelectrons. Only the electrons that originate from within tens of angstroms below the solid surface will manage to leave the surface without energy loss [22].

3. Methods

3.1 Experimental Setup

3.1.1 X-ray Photoelectron Spectroscopy

As previously introduced, XPS is the technique employed to perform this research project. Specifically, the analysis was carried out with an Near Ambient Pressure XPS (NAP-XPS). X-rays impinge on to the sample in the measurement chamber. A fraction of the photoelectrons that are ejected from the sample are collected by the analyzer cone and directed to the hemispherical analyzer, where electrons are analyzed. Specifically, the analyzer that we work with is the SCIENTA HiPP-3 analyzer, an electron spectrometer developed for XPS samples at near-ambient pressure ranging from tens of millibars down to UHV conditions.

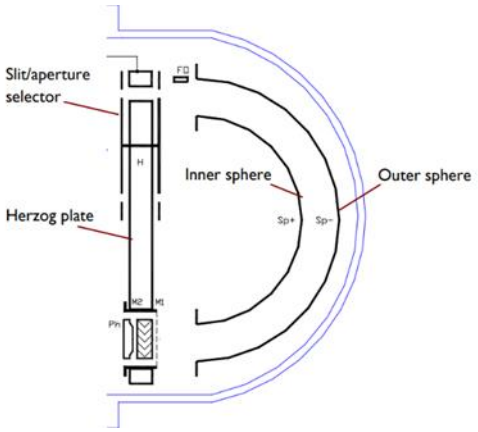

Figure 5: Schematic overview of the SCIENTA HiPP-3 from the device's manual.

The spectrometer will only accept electrons in a fixed energy window, known as the pass energy. The energy of the incoming electrons is tuned by an electrostatic field created between the inner and outer space to fit this energy window. The spectra that is shown in the SES program is therefore made up by the accepted electrons with the chosen pass the energy.

The monochromatic X-rays are generated by creating a potential gap between an aluminum anode and a cathode. A current is generated by a separate low voltage circuit on a filament at the cathode side. The thermionic emission effect will induce the release of electrons from the filament. Due the potential gap, the electrons will be accelerated to the Al anode. The bombarding of electrons towards the aluminum anode induce the release of X-rays [23].

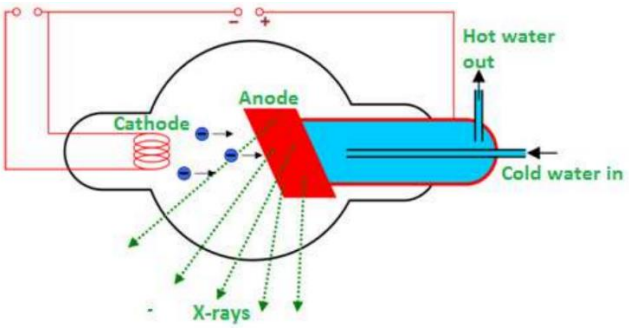

Figure 6: X-ray production process [23].

After their generation, the X-rays imping onto a quartz crystal that works as a diffraction grating, reflecting monochromatic X-rays of 1486.7 eV. The X-ray source used for this research employs a monochromatic Al Kα source (hν = 1486.6 eV) operating at a filament current of 2.4 A, emission current of 20 mA, and anode voltage of 12.5 kV. The X-ray source is separated from the measuring chamber by a silicon-nitride window. This separation allows to operate the X-ray source during exposure at elevated pressures.

3.1.2 Cracker

Molecular hydrogen was dissociated making use of the Oxford Thermal Gas Cracker TC-50. The cracker provides the capability of dissociation of gases and thus of generating a stream of atomic, low energy and highly reactive species. The working principle is filament electron-beam-induced heating of a metallic capillary through which the gas is passed before entering the vacuum chamber. Molecules

will be thermally dissociated when hitting the walls of the hot capillary. The catalytic nature of the capillary lowers substantially the otherwise high temperatures and power necessary to achieve dissociation. It allows for max operation at 65W and 1000ºC instead of the usual filament cracker of 400W and 2500ºC. Molecular hydrogen is effectively cracked at 55W. Specifically, the cracker operates with a ThO_2 coated tungsten filament and an catalytic capillary, through which a pressure of $2.5 \cdot 10^{-5} mbar$ of hydrogen is flowed (flow rate of 0.3 sccm).

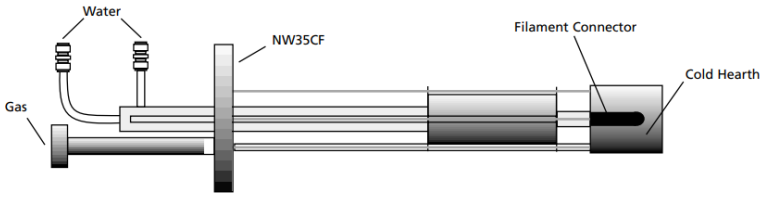

Figure 7: TC50 Thermal Cracker from the device's manual.

3.2 Experimental Approach

3.2.1 Sample preparation

Working with ultra-high vacuum requires careful sample preparation. To study the reduction process ruthenium single crystal (Ru(0001)) was cleaned in a sequential ultrasonic bath of acetone and isopropyl alcohol. High temperatures were employed to perform the experiments, therefore to mount the Ru on to the sample plate two tantalum strips with bolts were used to secure the sample.

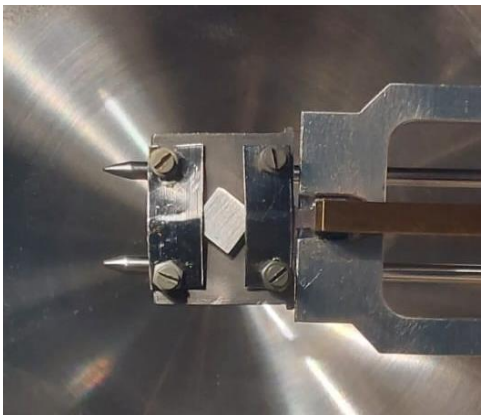

Figure 8: Ruthenium single crystal mounted onto the sample plate inside the measurement chamber of the XPS.

Inside the measurement chamber the Ru(0001) was annealed in UHV at 600ºC with a radiative heater for 1h to allow for full recovery of the crystal structure; the temperature was measured with a thermocouple. Oxidation of the Ru(0001) was performed at 400ºC at an oxygen pressure of 5.0×10^{-5} mbar for approximately 2h. This yields a ruthenium oxide layer of 2-4nm.

3.2.2 Measurement Procedure

To perform the measurements, first the X-ray source is switched on. Next, the sample's position is mechanically modified to find the optimal distance between the sample and the XPS cone to maximize

the number of photoelectrons detected. Once the optimal position is found, the desired spectrum can be recorded, consisting on intensity (amount of photoelectrons detected) vs binding energy.

The first recorded spectrum is a survey (1100-0eV binding energy) at a pass energy of 500 eV, which is a broad scan that is used to identify the elements present in the sample. This step is important to identify if there is any contaminant in the sample that are not wanted (F, Zn). Once the main elemental composition has been determined, narrower detailed core level spectra of the chosen atomic species of interest are taken. Being Ru3d and O1s spectra for this research. Spectra at a pass energy of 300 eV with 4 frames and step size 100meV is used to characterize the amount of elements present in the sample. A high-resolution spectra at a pass energy of 100 eV with 4 frames, step size of 50 meV is used to carefully track the evolution of the species. This research is performed taking in situ measurements, these parameters allow for acquisition of spectra of high intensity with short time resolution (3.5 minutes between consecutive spectra).

3.2.3 Data analysis

The obtained spectra are analyzed using kolXPD, a peak fitting program.

1- Ruthenium fit

To fit Ru the following steps are taken. Shirley background is implemented to subtract the background. Ru3d has two peaks due to the spin-orbit coupling, $Ru3d_{3/2}$ and $Ru3d_{5/2}$. The ratio between this two peaks is 3:2, this dependence is fixed in the parameters. The two peaks have a distance between them of 4.192 eV, which is also fixed in the fitting parameters. Fixing the relative position and area ratios will ensure that if the obtained fit adjusts correctly to the experimental data, the species that are speculated to be present are the correct ones.

Metallic ruthenium is fitted with a convolution of a Cauchy-Lorentz distribution and a Gaussian distribution (Voigt peak). Ruthenium oxide is fitted with two Doniac-Sunjic-Gaussian convoluted (DSG) asymmetric peaks due to its conductor behavior. In addition, ruthenium oxide has a characteristic plasmon, an energy loss feature, that is fitted with a Voigt peak.

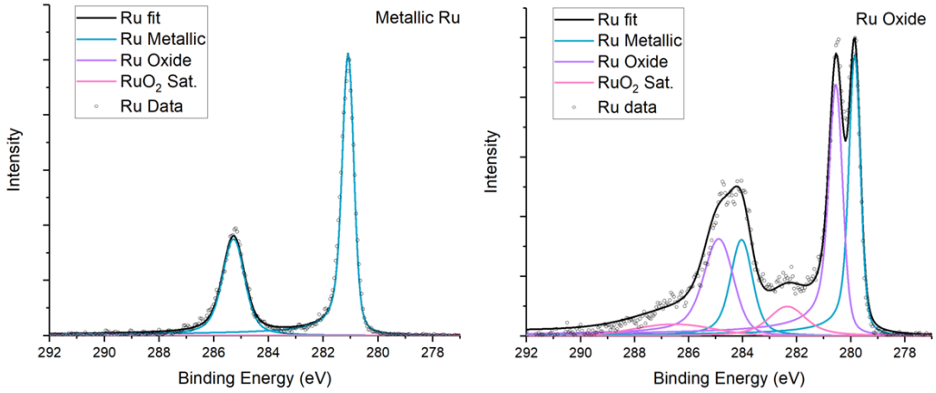

Figure 9: XPS spectra of a) Metallic ruthenium 3d and b) Ruthenium dioxide 3d.

2- Oxygen fit

To fit oxygen the same procedure is followed. O1s only has one peak as s orbitals do not present spin-orbit coupling and therefore there is no constraint on area ratios. Reviewing the reported binding energy of different species in literature allows for identification of the peaks obtained. The species identified have to be consistent with the ones expected in the studied process. In this research project reduction is studied, therefore OH, H_2O and RuO_2 is expected and supported by literature [14, 24, 25]. It is of high importance to account for and fix the relative position between the different species peaks. These 3

species provide a good fit to the recorded spectra. Without the introducing of a 3rd peak, related to water species, the error associated to the fit of the spectrum on Figure 10 is significant. This observation is relevant in the framework of ruthenium reduction employing molecular vs atomic hydrogen.

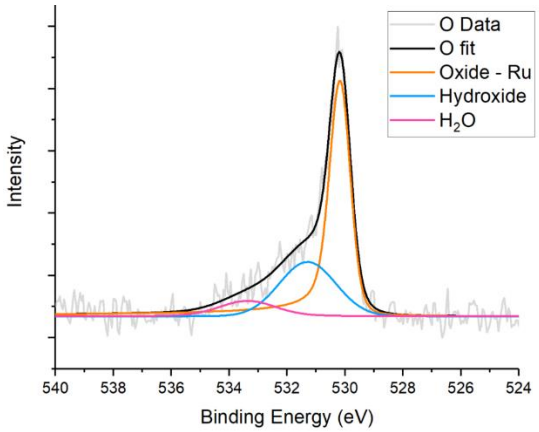

Figure 10: XPS spectra of Oxygen 1s.

3.2.4 Ruthenium oxide layer determination

To account for the ruthenium oxide layer thickness the formula reported by A. Jablonski and J. Zemek in [26] is used. The formula provides with the oxide layer thickness *t* in nm by relating the intensity ratio of the oxide (I_{RuO_2}) and the ruthenium peak (I_{Ru}), the atomic density ratios (M), the inelastic mean free path (λ) and the detection angle with respect to the surface (α):

$$t = \lambda \cos\alpha \ln\left(\frac{I_{RuO_2}}{I_{Ru}} \frac{M_{Ru}\,\lambda^{S}_{Ru}}{M_{RuO_2}\,\lambda^{l}_{RuO_2}} + 1\right) \quad (5)$$

Formula (5) makes use of the approximation that the inelastic mean free path (IMFP) of photoelectrons emitted in the overlayer and moving in the overlayer material is similar as the IMFP of the photoelectrons emitted in substrate and moving in the overlayer. This approximation is applicable for the case of ruthenium and ruthenium oxide.

4. Considerations & Acknowledgements

The experimental data obtained during this research project presents clear differences in the RuO_2 reduction when applying atomic and molecular hydrogen. Moreover, a deep study about the evolution and role of the oxygen species involved in the reduction is performed. These results will be addressed in the article included in section 5 of this thesis. This research will be supported in the future by other techniques such as, low-energy ion scattering spectroscopy (LEIS) and scanning tunneling microscopy. The influence of the ion-surface interaction along with plasma effects is also planned to be addressed.

I would like to thank ARCNL for providing me with the unique opportunity of conducting and contributing to state of the art research on Surface Science, executed in an exceptional experimental environment. I consider ARCNL to be an outstanding international community-based center, from which I have deeply learnt from and profited of during the development of this project. I would further like to thank the whole Materials & Surface Science for EUVL group, from group leader to Ph.D. candidates and technician. They have been extremely welcoming, educative and fun to work with, making this experience very enjoyable and didactic. I specifically want to express my gratitude towards Roland Bliem, as my supervisor, and Stefan van Vliet, as my daily supervisor, for their excellent supervision, guidance and teaching. I can confidently say I wouldn't have grown and learned as much as I have these past 10 months without their constant feedback, support and mentorship. As a result of this internship I am more excited than ever and feel well-equipped to pursue a career in Materials and Surface Science.

References

[1] Hitachi High-Tech Corporation, 2022, "History of semiconductors", https://www.hitachi-hightech.com/global/products/device/semiconductor/history.html#:~:text=The%20semiconductor%20industry%20grew%20rapidly,Fairchild%20Semiconductor%20in%20the%20US.

[2] Gordon E Moore. 'Progress in digital integrated electronics'. In: vol. 21. Washington, DC, 1975, pp. 11–13.

[3] M Mitchell Waldrop. 'The chips are down for Moore's law'. In: Nature News 530 (7589 2016),p. 144002E.

[4] van de Kerkhof, M. A. ; Benschop, J. P. H. ; Banine, V. Y. "Lithography for now and the future. In: Solid-state electronics. 2019 "; Vol. 155. pp. 20-26.

[5] Jan van Schoot et al. "The future of EUV lithography: continuing Moore's Law into the next decade". In: vol. 10583. International Society for Optics and Photonics, 2018, 105830R.

[6] Benschop, Jos ; Banine, Vadim ; Lok, Sjoerd ; Loopstra, Erik. "Extreme ultraviolet lithography : Status and prospects". Journal of Vacuum Science and Technology B: Microelectronics and Nanometer Structures. 2008 ; Vol. 26, No. 6. pp. 2204-2207.

[7] Arie J. Den Boef. "Optical wafer metrology sensors for process-robust CD and overlay control in semiconductor device manufacturing". In: Surface Topography: Metrology and Properties 4 (2 Feb. 2016), p. 023001.

[8] E. Louis, A.E. Yakshin, T. Tsarfati, F. Bijkerk, "Nanometer interface and materials control for multilayer EUV-optical applications", Progress in Surface Science, Volume 86, Issues 11–12, 2011, Pages 255-294.

[9] van de Kerkhof, Marcus & Yakunin, Andrei & Astakhov, Dmitry & Kampen, Maarten & Horst, Ruud & Banine, Vadim. (2021). "EUV-induced Hydrogen Plasma : Pulsed Mode Operation and Confinement in Scanner". Journal of Micro/Nanopatterning, Materials, and Metrology, Volume 20, id. 033801 (2021).

[10] Dolgov, Alexandr & Lee, Chris & Bijkerk, F. & Abrikosov, Alex & Krivtsun, Vladimir & Lopaev, Dmitry & Yakushev, O. & Kampen, M.. (2018). "Plasma-assisted oxide removal from ruthenium-coated EUV optics". Journal of Applied Physics. 123. 153301. 10.1063/1.5006771.

[11] Sasa Bajt, Henry N Chapman, Nhan Nguyen, Jennifer B. Alameda, Jeffrey C. Robinson, Michael E. Malinowski, Eric Gullikson, Andy Aquila, Charles Tarrio, and Steven Grantham "Design and performance of capping layers for EUV multilayer mirrors", Proc. SPIE 5037, Emerging Lithographic Technologies VII, (16 June 2003).

[12] Nishiyama, Iwao et al. "Reduction of oxide layer on Ru surface by atomic-hydrogen treatment." Journal of Vacuum Science & Technology B 23 (2005): 3129-3131.

[13] H2 D. Ugur, A. J. Storm, R. Verberk, J. C. Brouwer, and W. G. Sloof . "Kinetics of Reduction of a RuO2(110) Film on Ru(0001)" . The Journal of Physical Chemistry C 2012 116 (51), 26822-26828.

[14] D. Ugur, A.J. Storm, R. Verberk, J.C. Brouwer, W.G. Sloof, "Kinetics of reduction of a RuO2(110) film on Ru(0001) by atomic hydrogen", Microelectronic Engineering, Volume 110, 2013, Pages 60-65.

[15] Over, Y.B. He, A. Farkas, G. Mellau, C. Korte, M. Knapp, M. Chandhok, C. Fang,J. Vac. Sci. Technol. "Long-term stability of Ru-based protection layers in extreme ultraviolet lithography: A surface science approach", Journal of Vacuum Science & Technology B: Microelectronics and Nanometer Structures Processing, Measurement, and Phenomena 25, 1123-1138, (2007).

[16] Y. B. He, M. Knapp, E. Lundgren, and H. Over. “Ru(0001) Model Catalyst under Oxidizing and Reducing Reaction Conditions: In-Situ High-Pressure Surface X-ray Diffraction Study”. The Journal of Physical Chemistry B 2005 109 (46), 21825-21830.

[17] W. F. Lin, M. S. Zei, Y. D. Kim, H. Over, and G. Ertl. “Electrochemical versus Gas-Phase Oxidation of Ru Single-Crystal Surfaces”. The Journal of Physical Chemistry B 2000 104 (25), 6040-6048.

[18] Ping Liu, James T. Muckerman, and Radoslav R. Adzic , "Adsorption of platinum on the stoichiometric RuO2(110) surface", J. Chem. Phys. 124, 141101 (2006).

[19] Encyclopedia of Materials: Science and Technology, ISBN: 978-0-08-043152-9, p. 8991-8996.

[20] Pais, A. (1979), “Einstein and the Quantum Theory”. Reviews of Modern Physics, 51, 863-914.

[21] U. Burghaus, in New and Future Developments in Catalysis, 2013, section 2.3.3.1.

[22] Mahuvava, Courage & du plessis, Freek. (2015). “Monte Carlo evaluation of the dose perturbation effect of hip prostheses for megavoltage photon radiotherapy”. Physica Medica. 31. S7.

[23] Prabhu, Sangeetha & Naveen, Divya & Bangera, Sandhya & Bhat, B. (2020). “Production of X-RAYS using X-RAY Tube”. Journal of Physics: Conference Series. 1712.

[24] J. Hrbek, “Coadsorption of oxygen and hydrogen on ruthenium(001): blocking and electronic effects of preadsorbed oxygen”, The Journal of Physical Chemistry 1986 90 (23), 6217-6222.

[25] Sugimoto, W., Ireysa, G., Ota, Ki., Savinell, R.F. (eds) (2014). “Ruthenium Oxides as Supercapacitor Electrodes”. Encyclopedia of Applied Electrochemistry. Springer, New York, NY.

[26] Jablonski, A. and Josef Zemek. “Overlayer thickness determination by XPS using the multiline approach.” Surface and Interface Analysis 41 (2009).

5. Article

Effect of atomic and molecular hydrogen on the reduction process of ruthenium dioxide

Gaining insights into the reduction process of ruthenium dioxide by atomic hydrogen is relevant for the optimization of the lifetime of the optics of extreme ultraviolet nanolithography machines. In this article we report an in situ X-ray photoelectron spectroscopy (XPS) study of the different effect that atomic vs molecular hydrogen has on the reduction of ruthenium dioxide. The results presented in this paper demonstrate that reduction of RuO_2 using H* leads to a more effective and faster reduction of the oxide layer than through H_2. We further report a detailed study of the evolution of the oxygen species involved in this reaction, oxide, hydroxide, and adsorbed water. A systematic difference of the evolution of these 3 oxygen species during reduction with H* and H_2 is identified.

1. Introduction

One of the major challenges that extreme ultraviolet nanolithography (EUVL) faces is the limited lifetime of the multilayer optics due to contaminant agents present inside the lithography machine. To minimize this problem a ruthenium (Ru) coating is used as an oxidation resistant capping layer for the Si/Mo multilayer mirrors [1]. Under intense irradiation with EUV light in air, the Ru protective layer would oxidize. To avoid this situation a reducing environment is created inside the machine. This environment is employed to fight the effect of the contaminants and maintain self-cleaning conditions for the optics [2]. Nevertheless, over time oxidation of the Ru protective layer takes place. This process leads to a decrease in the reflectivity and, hence, a shorter lifespan of the optics. Removal of the ruthenium oxide layer is key to optimizing the performance of EUV lithography machines. Reduction of such oxide layer through exposure to hydrogen has been previously reported as a potential cleaning mechanism for the optics [3,4]. However, the detailed steps of the reduction process are not fully understood yet. Gaining insights into the stages of the reduction and its optimal conditions would contribute to the development of more effective cleaning methods of the optics of the EUV machines.

The interaction of hydrogen with metal oxides is a topic of high relevance due to the many industrial processes in which it is involved in; heterogeneous catalysis such as methanol synthesis [5], manufacturing of electronic devices like solid-state thin-film supercapacitors [6] among others. The presence of hydrogen on metal oxides surfaces has a pronounced influence on their chemical, structural and magneto-electrical properties [7]. The interaction of hydrogen with ruthenium oxide is a particularly relevant example in the fields of catalysis and semiconductor manufacturing. Ruthenium dioxide (RuO_2) serves as an excellent oxidation catalyst [8,9]. It is specifically suitable for low-temperature dehydrogenation of small molecules in heterogeneous catalysis such as NH_3, HCl and methanol [10].

In an oxygen-rich environment, single crystalline Ru(0001) oxidizes, forming a rutile crystal structure that grows epitaxially on the metal surface [11]. Under certain temperature, hydrogen pressure and exposure time, hydrogen will induce the reduction of this oxide layer. The reduction mechanism of RuO_2 has been studied in literature [4, 11-13] making use of scanning tunneling microscopy (STM), temperature-controlled reaction (TPR), surface X-ray diffraction (SXRD), low-energy electron diffraction (LEED), high resolution core level shift spectroscopy (HRCLS) among other techniques, in combination with DFT calculations [14]. These studies report that RuO_2 reduction takes place in 3 stages. Initially, the formation of surface hydroxyl groups (OH) takes place, for H_2 previous dissociation of the molecule occurs. Upon the addition of another hydrogen to a hydroxyl group, the formation of a water molecule (H_2O) takes place. Re-accommodation of the H_2O to another location in the lattice follows. In this new location it is thermally desorbed [4, 11]. This process creates surface oxygen vacancies that trigger oxygen diffusion from deeper layers to the surface. This

exchange mechanism enables the continuation of RuO_2 reduction [11,15].

The reduction process varies for molecular (H_2) and atomic hydrogen (H*) [11,15]. Previous studies report the reduction of stoichiometric RuO_2(110) film by H_2 at pressure of 1×10^{-6} mbar in 3 temperature ranges, 100-200°C, 200-300°C and above 300°C. The study establishes that the reduction stages of RuO_2 through H_2 is highly dependent on the temperature, only presenting full oxide removal above 200°C [11]. The reduction efficiency of RuO_2(110) film by H* has been reported to be an order of magnitude higher than reduction by H_2 under similar conditions [15]. In the temperature range of 60-200°C, atomic hydrogen reduction starts with an initial slow rate followed by a fast reduction where the majority of the oxide is removed within minutes of exposure to hydrogen. Nevertheless, full reduction of the oxide layer has not been observed when employing H* [3, 15]. The role that different oxygen species play in the reduction process has not been resolved.

Acquiring understanding of the systematic difference between the interaction of atomic and molecular hydrogen with RuO_2 during reduction is highly relevant for optimization of its industrial applications, not only for the EUVL protective layer, but also for its catalytic role. This article presents the study of RuO_2 reduction using H* vs H_2 at close to room temperature and higher temperatures (up to 85°C). Moreover, we present a detailed study of the evolution of the oxide, hydroxide, and adsorbed water employing molecular H* vs H_2. This research was conducted making use of near-ambient pressure X-ray photoelectron spectroscopy (XPS).

2. Methods

Sample preparation: Ruthenium single crystal (Ru(0001)) was cleaned in a sequential ultrasonic bath of acetone and isopropyl alcohol. The Ru(0001) was annealed in ultra-high vacuum (UHV) at 600°C with a radiative heater for 1h to allow for full recovery of the crystal structure; the temperature was measured with a thermocouple. Oxidation of the Ru(0001) was performed at 400°C at an oxygen pressure of 5.0×10^{-5} mbar for approximately 2h. This yields a ruthenium oxide layer of 2-4nm, calculated from XPS peak intensities [16].
X-ray photoelectron spectroscopy: The step-by-step reduction process was investigated making use of near-ambient pressure X-ray photoelectron spectroscopy in a UHV set up (base pressure under 1.0×10^{-9} mbar). The analysis was carried out with a HiPP-3 spectrometer using a monochromatic Al Kα X-ray source (1486.6 eV). The HiPP-3 analyzer is used with a 0.8 mm cone and a slit setting of 1.0 mm. XPS peak fitting is performed using KolXPD. Survey was measured at a pass energy of 500 eV, Ru3d and O1s spectra at a pass energy of 300 eV and high-resolution spectra at a pass energy of 100 eV, see Fig. 1.
Exposure: The reduction was performed leaking in a pressure of 2.5×10^{-5} mbar of hydrogen. Atomic hydrogen is generated making use of Oxford Thermal Gas Cracker TC-50 operated at 55W. The use of the cracker increases the sample surface temperature to 40°C due to radiative heating of the sample by the cracker element.

3. Results and Discussion

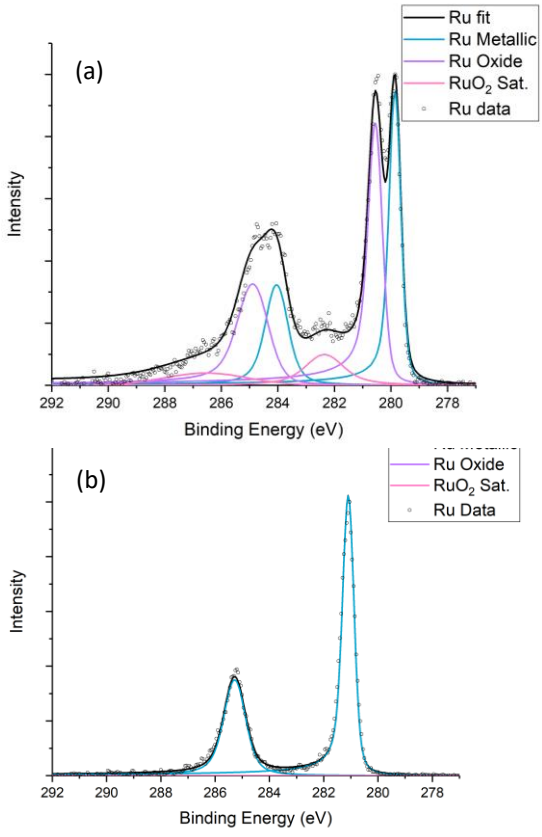

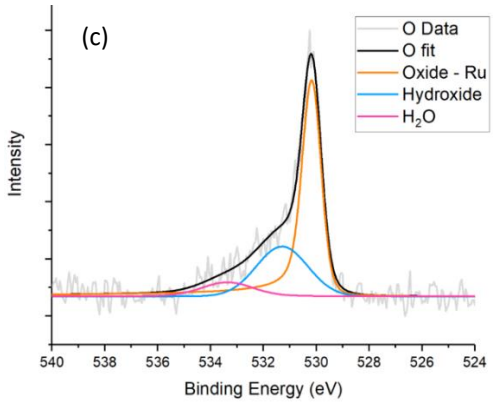

FIG. 1. XPS spectra at pass energy 100 eV of (a) Metallic Ru3d. (b) Ru3d oxide. (c) O1s

Reduction of RuO_2

The oxide layer thickness as a function of time using H* and H_2 at 40°C and 85°C is depicted in Fig. 2. The dark green triangles, corresponding to data in H_2 at 40°C, show no change in thickness with time. The dark blue triangles, representing H* at 40°C, show a slow decrease of the oxide layer thickness. The light green circles, corresponding to H_2 at 85°C, show a slow decrease of the oxide layer in the initial stage, followed by a faster reduction that does not remove the oxide completely. The light blue circles, representing H* at 85°C, show an immediate fast decrease until no oxide layer is left.

From Fig. 2 it can be inferred that when applying H_2 at 40°C no reduction of the ruthenium oxide layer takes place. Increasing the temperature to 85°C, H_2 induced a reduction of 2.45 nm in the span of 203 minutes without achieving full reduction. Employing H* at 40°C, a reduction of 0.96 nm took place in the span of 171.5 minutes without achieving full reduction. At a higher temperature of 85°C, H* fully reduced a layer of 3.54 nm thickness An overview is provided in Table 1.

Comparing the effect of H_2 vs H* we conclude that close to room temperature (40°C), the reduction of RuO_2 is only possible through H*. At higher temperatures, significant reduction occurs with H_2 but proceeds faster for H*. Only H* leads to full reduction of RuO_2 at 85°C (under the span of 215 min). Even at higher temperatures than 85°C, full reduction of the RuO_2 layer through exposure to H* has not been previously reported in literature. Nevertheless, the presence of a non-negligible fraction of ions with energies of several hundreds of eV in the hydrogen beam cannot be ruled out.

Overall, reduction with H* is faster and more effective than through H_2, which is in agreement with literature [15] assuming that the flux of hydrogen atoms is equal in both experiments (within experimental error).

Reduction of RuO_2 is sped up by temperature. This observation indicates a temperature dependence of the oxide layer stability, proving that it is an oxygen diffusion limited process, as reported in literature [11]. This point will be further addressed in the section *Oxygen species development during multiple reduction and heating steps.*

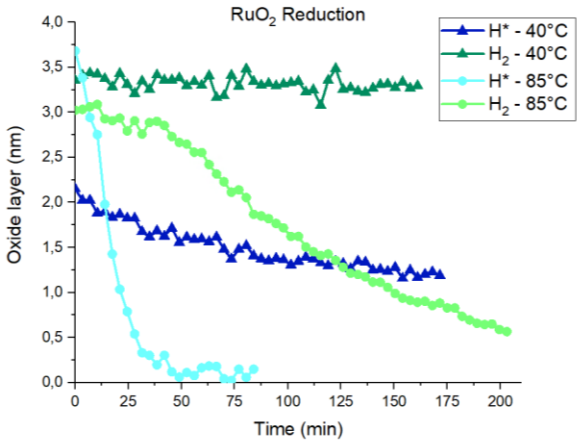

FIG. 2. Green lines represent the reduction performed with H_2, blue lines with H*. Triangles represent the experiments performed at 40°C, circles at 85°C .

	Start oxide layer (nm)	Final oxide layer (nm)	nm reduced	Time (min)	Full reduction?
H_2-40°C	3.35	3.29	0.6	161	No
H_2-85°C	3.02	0.57	2.45	203	No
H*-40°C	2.15	1.19	0.96	171.5	No
H*-85°C	3.69	0.15	3.54	84	Yes

Table 1. Data of the oxide layer reduction for the different conditions.

Oxygen species

During the course of the reduction, detailed O 1s spectra were recorded. The evolution of the different oxygen species is illustrated in Fig. 3. As reported in literature [15, 17, 18], three different species are identified, Ru-OH groups, oxide species and H_2O.

Fig. 3(a) and 3(c) show the evolution of the components in the O 1s region when reducing with H_2 at 40°C and 85°C, respectively. No change occurs in Fig. 3(a) as no reduction of the oxide layer takes place. For the reduction with H_2 at 85°C, a decrease of the intensity of oxide and hydroxide is observed, whereas no clear signature of water is discernible.

Fig. 3(b) and 3(d) show the evolution when reducing with H* at 40°C and 85°C respectively. Fig. 3(b) presents a fast decrease of the oxide species, dropping under the OH species at the 28th minute mark. A first increase in the H_2O species is observed, followed by a maintained non-zero value, 4-21% of the total oxygen signal. Employing H* at 85°C leads to a fast evolution of the species maintaining the previously reported tendency. The oxide species decreases and at the 21st minute mark it falls under the OH intensity. The H_2O species increases and remains present while the reduction is taking place. The possibility that the H_2O at elevated temperature is not observed because of shorter residence time is contemplated.

These experiments reveal systematically different behavior of the three species of oxygen when reduced with H_2 vs H* and close to room temperature vs at an elevated temperature of 85°C. The sharp intensity drop of the oxide species under the OH component, Fig. 3 (b) and (d), is only observed when making use of H*. This behavior suggests a change in the RuO_2 surface topography, attributed to the removal of the oxygen through the desorption of H_2O and the formation of Ru islands, previously reported in the literature [19-21]. The presence of adsorbed H_2O at low temperatures is observed, indicating a varying presence of water with temperature. The desorption of H_2O is not the rate-limiting step as it desorbs at 27°C [15]. These experiments provide in situ spectroscopic evidence that the H_2O species is present. Furthermore it illustrates the gradual oxide surface conversion to the different structure presenting Ru islands.

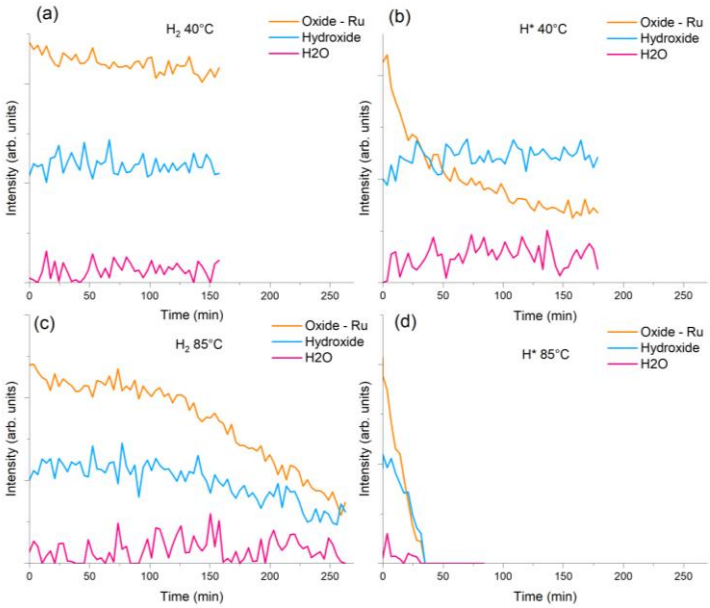

FIG. 3. Evolution of the three oxygen species observed in XPSduring in situ reduction of the RuO_2 layer. a) H_2 at 40°C, b) H* at 40°C, c) H_2 at 85°C, d) H* 85°C. The orange curve represents the oxygen attributed to the oxide, the blue curve to hydroxides (OH) and the pink curve to H_2O.

Oxygen species development during multiple reduction and heating steps

The evolution of the three oxygen species was followed in a long experiment with multiple reduction and heating steps, depicted in Fig. 4. H* was leaked at 40°C during the first 164.5 min. At minute 168, the hydrogen flow was closed and allowed for the chamber to reach UHV again before the next step to ensure the absence of hydrogen in the camber. The sample was heated up in UHV to 100°C from 168 until 192.5 min. The sample remained at 100°C for 87.5 minutes. The system was cooled down until 40°C and a second atomic hydrogen reduction was performed under the same conditions as before from 301 min to 378 min. During the first 164.5 min, a first reduction takes place where the oxygen species develop as previously described, see also Fig 3(b). The oxide species decreases fast until a certain point where its intensity falls under that of the OH species. A significant signal from H_2O is observed. During the following annealing step

in the absence of hydrogen at 100°C, the oxide species increases and the OH species sharply decreases below the oxide one. The H_2O intensity drops to zero. During the second atomic hydrogen reduction at 40°C the pattern is repeated; again the oxide intensity drops below the OH species and an increase in water species is observed.

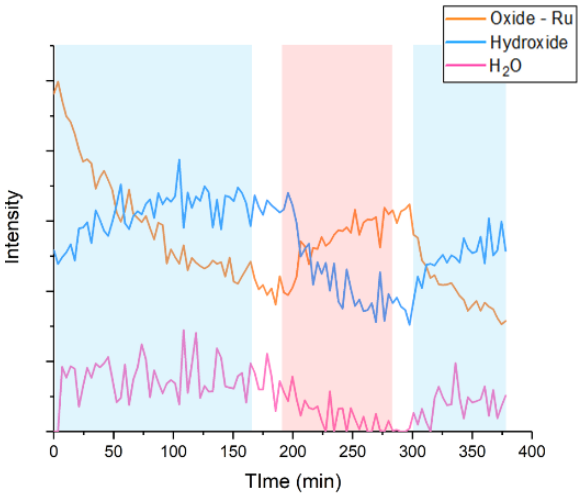

FIG. 4. Evolution of the three oxygen species observed in XPS during in situ experiment with multiple reduction and heating steps. The blue shade corresponds to the atomic hydrogen reduction and the red shade corresponds to the sample at 100°C in UHV.

The first reduction illustrates the behavior that is only observed when using H* , attributed to the formation of the Ru islands, as previously introduced [19-21]. It is observed that the 3 oxygen species present a different evolution trend after some time exposed at 100°C. At this stage, the H_2O and the OH species decrease indicating their desorption taking place as a thermally induced effect. Simultaneously to this process, the increase of the oxide species in the absence of hydrogen flux at 100°C is attributed to the also decomposition of OH followed by desorption of H_2, leading to more oxide on the surface. This increase in oxygen could also suggest the existence of RuO_2 buried in deeper layers and the temperature-induced oxygen diffusion to the surface. This exchange mechanism between the oxygen from the bulk and the surface oxygen vacancies created in the reduction process has been previously reported with other techniques, addressed in the introduction [22,23]. Nevertheless, the data obtained in this experiment does not suffice to state that this is the case in our experiment.

When hydrogen is leaked into the chamber again, the reduction continues further following the previously reported process. This indicates that a fresh surface has been restored.

4. Conclusions

The results presented in this research do not only shows a faster, more effective reduction of RuO_2 with H*, but also demonstrates the systematic difference of the evolution of the 3 oxygen species involved in the reduction process of RuO_2 with H* and H_2. Such differences point to a direct influence of the nature of the reducing species on the resulting morphology of the ruthenium. We report the presence of adsorbed H_2O at low temperatures, indicating a varying presence of water with temperature during reduction. The introduced experiments present a first in situ near ambient pressure XPS study on the 3 species of oxygen participating in the reduction of RuO_2, illustrating temperature-dependent surface evolution. The gained insights into the stages and the optimal conditions for the reduction of RuO_2 shows potential for the optimization and maintenance of the self-cleaning conditions for the ruthenium protective coating of the optics of EUVL machines; it further shines light on to hydrogen-driven reduction of metal oxides relevant in a variety of industrial applications.

5. Acknowledgments

This research has been conducted at the Advanced Research Center for Nanolithography, a public-private partnership of the Univiersiteit van Amsterdam, the Vrije Universiteit Amsterdam, the Dutch Research Council (NWO) and the semiconductor equipment manufacturer ASML.

References

[1] Sasa Bajt, Henry N Chapman, Nhan Nguyen, Jennifer B. Alameda, Jeffrey C. Robinson, Michael E. Malinowski, Eric Gullikson, Andy Aquila, Charles Tarrio, and Steven Grantham. "Design and performance of capping layers for EUV multilayer mirrors", Proc. SPIE 5037, Emerging Lithographic Technologies VII, (16 June 2003).

[2] van de Kerkhof, Marcus & Yakunin, Andrei & Astakhov, Dmitry & Kampen, Maarten & Horst, Ruud & Banine, Vadim. "EUV-induced Hydrogen Plasma : Pulsed Mode Operation and Confinement in Scanner''. Journal of Micro/Nanopatterning, Materials, and Metrology, Volume 20, id. 033801 (2021).

[3] Nishiyama, Iwao et al. "Reduction of oxide layer on Ru surface by atomic-hydrogen treatment." Journal of Vacuum Science & Technology B 23, 3129-3131, (2005).

[4] Over, Y.B. He, A. Farkas, G. Mellau, C. Korte, M. Knapp, M. Chandhok, C. Fang,J. Vac. Sci. Technol. "Long-term stability of Ru-based protection layers in extreme ultraviolet lithography: A surface science approach", Journal of Vacuum Science & Technology B: Microelectronics and Nanometer Structures Processing, Measurement, and Phenomena 25, 1123-1138, (2007) .

[5] Genger, T., Hinrichsen, O. & Muhler, M. "The temperature-programmed desorption of hydrogen from copper surfaces''. Catalysis Letters 59, 137–141 (1999).

[6] Y.S Yoon, W.I Cho, J.H Lim, D.J Choi. "Solid-state thin-film supercapacitor with ruthenium oxide and solid electrolyte thin films". Journal of Power Sources, 101, 126 (2001).

[7] Kineshma Munbodh, Felio A. Perez, and David Lederman , "Changes in magnetic properties of Co/Pd multilayers induced by hydrogen absorption", Journal of Applied Physics 111, 123919 (2012).

[8] Iqbal, Muhammad & Abdel-Magied, Ahmed & Abdelhamid, Hani & Olsén, Peter & Shatskiy, Andrey & Zou, Xiaodong & Åkermark, Björn & Kärkäs, Markus & Johnston, Eric. "Mesoporous Ruthenium Oxide: A Heterogeneous Catalyst for Water Oxidation. ACS Sustainable Chemistry & Engineering". (2017).

[9] Over, Herbert & Kim, Yousoo & Seitsonen, Ari & Wendt, Stefan & Lundgren, Edvin & Schmid, M. & Varga, Peter & Morgante, A. & Ertl, Gerhard. "Atomic-Scale Structure and Catalytic Reactivity of the RuO2(110)". Surface Science. 287. 1474-1476. (2000).

[10] Herbert Over. "Surface Chemistry of Ruthenium Dioxide in Heterogeneous Catalysis and Electrocatalysis: From Fundamental to Applied Research". Chemical Reviews 112 (6), (2012).

[11] D. Ugur, A. J. Storm, R. Verberk, J. C. Brouwer, and W. G. Sloof . "Kinetics of Reduction of a RuO2(110) Film on Ru(0001)" . The Journal of Physical Chemistry C, 116 (51), 26822-26828, (2012).

[12] Y. B. He, M. Knapp, E. Lundgren, and H. Over. "Ru(0001) Model Catalyst under Oxidizing and Reducing Reaction Conditions: In-Situ High-Pressure Surface X-ray Diffraction Study". The Journal of Physical Chemistry B , 109 (46), 21825-21830, (2005).

[13] W. F. Lin, M. S. Zei, Y. D. Kim, H. Over, and G. Ertl. "Electrochemical versus Gas-Phase Oxidation of Ru Single-Crystal Surfaces". The Journal of Physical Chemistry B, 104 (25), 6040-6048, (2000).

[14] Ping Liu, James T. Muckerman, and Radoslav R. Adzic , "Adsorption of platinum on the stoichiometric RuO2(110) surface", J. Chem. Phys. 124, 141101 (2006).

[15] D. Ugur, A.J. Storm, R. Verberk, J.C. Brouwer, W.G. Sloof, Kinetics of reduction of a RuO2(110) film on Ru(0001) by atomic hydrogen, Microelectronic Engineering, Volume 110, Pages 60-65, (2013).

[16] Jablonski, A. and Josef Zemek. "Overlayer thickness determination by XPS using the multiline approach." Surface and Interface Analysis 41 (2009).

[17] J. Hrbek. “Coadsorption of oxygen and hydrogen on ruthenium(001): blocking and electronic effects of preadsorbed oxygen”.The Journal of Physical Chemistry, 90 (23), 6217-6222, (1986).

[18] Sugimoto, W, Kreysa, G., Ota, Ki., Savinell, R.F. (eds). “Ruthenium Oxides as Supercapacitor Electrodes”. Encyclopedia of Applied Electrochemistry. Springer, New York, NY. (2014).

[19] Lj. Atanasoska, W.E. O'grady, R.T. Atanasoski, F.H. Pollak. “The surface structure of RuO2: A leed, auger and XPS study of the (110) and (100) faces”, Surface Science, Volume 202, Issues 1–2, 142-166, (1988).

[20] H. . Over, A.P. Seitsonen, E. Lundgren, M. Schmid, P. Varga, “Experimental and simulated STM images of stoichiometric and partially reduced RuO2(110) surfaces including adsorbates”, Surface Science, Volume 515, Issue 1, Pages 143-156, (2002).

[21] Over H, Knapp M, Lundgren E, Seitsonen AP, Schmid M, Varga P. “Visualization of atomic processes on ruthenium dioxide using scanning tunneling microscopy”. Chemphyschem. F 20;5(2):167-74, (2004).

[22] Knapp M, Crihan D, Seitsonen AP, Resta A, Lundgren E, Andersen JN, Schmid M, Varga P, Over H. “Unusual process of water formation on RuO2(110) by hydrogen exposure at room temperature”. J Phys Chem B. Jul 27;110(29):14007-10, (2006).

[23], Marcus Knapp, Daniela Crihan, Ari P. Seitsonen, and Herbert Over. “Hydrogen Transfer Reaction on the Surface of an Oxide Catalyst”, Journal of the American Chemical Society,127 (10), 3236-3237, (2005).